

# Scalable enhancement of graphene oxide properties by thermally driven phase transformation

Priyank V. Kumar<sup>1†</sup>, Neelkanth M. Bardhan<sup>1,2†</sup>, Sefaattin Tongay<sup>3</sup>, Junqiao Wu<sup>3</sup>, Angela M. Belcher<sup>1,2,4\*</sup> and Jeffrey C. Grossman<sup>1\*</sup>

**Chemical functionalization of graphene is promising for a variety of next-generation technologies. Although graphene oxide (GO) is a versatile material in this direction, its use is limited by the production of metastable, chemically inhomogeneous and spatially disordered GO structures under current synthetic protocols, which results in poor optoelectronic properties. Here, we present a mild thermal annealing procedure, with no chemical treatments involved, to manipulate as-synthesized GO on a large scale to enhance sheet properties with the oxygen content preserved. Using experiments supported by atomistic calculations, we demonstrate that GO structures undergo a phase transformation into prominent oxidized and graphitic domains by temperature-driven oxygen diffusion. Consequently, as-synthesized GO that absorbs mainly in the ultraviolet region becomes strongly absorbing in the visible region, photoluminescence is blue shifted and electronic conductivity increases by up to four orders of magnitude. Our thermal processing method offers a suitable way to tune and enhance the properties of GO, which creates opportunities for various applications.**

Graphene oxide (GO) is a versatile, solution-processable candidate material for next-generation, large-area, ultrathin electronics<sup>1,2</sup>, optoelectronics<sup>3</sup>, energy conversion and storage technologies<sup>4–7</sup>. GO is an atom-thick sheet of carbon functionalized with several oxygen-containing groups dominated by the epoxy and hydroxyl functional groups on the basal plane, with carboxyls and lactols at the sheet edges<sup>8</sup>. The ability to tune and spatially control the oxygen functionality in GO structures is a critical factor in opening up bandgaps comparable to those of silicon (~1 eV) for applications in electronics and photonics<sup>3,9</sup>. Such control is desirable for many future technologies based on green and sustainable catalysts<sup>10,11</sup>, metal/semiconductor composites<sup>12–15</sup> and chemical/biological sensors<sup>3</sup> that can utilize the rich and interactive oxygen framework in GO in a number of ways. However, the central issue currently limiting GO's direct deployment in these devices is the material's inherent chemical inhomogeneity and structural disorder caused by the harsh chemical environments employed during current synthesis protocols, and the inability to exercise spatial control over oxygen groups in these processes<sup>16–18</sup>. These limitations result in large optical gaps (~5.6 eV) and poor electronic conductivity that affect device performance unfavourably<sup>3,19,20</sup>. Given the high impact of controlled oxygen functionalization on the increasing number of applications that utilize GO, it is of prime importance to develop methods that preserve the oxygen functionality and yet enhance the optical and electronic properties.

A standard approach used to produce GO structures on a large scale is the Hummers method, which typically renders oxygen concentrations of 30–35 atomic per cent (at%)<sup>16</sup>. To date, a number of methods to improve the sheet characteristics of as-synthesized GO structures have been reported, but almost all of these improvements come at the expense of oxygen content. One such procedure

is to produce reduced GO (rGO) with 5–8 at% oxygen<sup>19,20</sup>. Alternatively, several groups have attempted careful hydrothermal treatments under alkaline or acidic conditions and achieved partial success in conserving oxygen functionality (15–20 at%) with improved sheet properties<sup>10,21–23</sup>. Other approaches include controlled chemical functionalization methods, such as dissociation of oxygen molecules in an ultrahigh vacuum to achieve selective epoxy functionalization<sup>24</sup>, the use of local reduction methods with nanometer resolution<sup>25</sup> and thermal annealing at 750 °C to produce graphene monoxide<sup>26</sup>. However, these techniques require expensive ultrahigh-vacuum equipment and high-temperature systems, which makes them less amenable to the large-scale processing of GO sheets. Also, high-throughput and easily scalable protocols that aim to enhance the sheet properties and still retain the oxygen content of as-synthesized GO are yet to be developed fully.

In this work, we demonstrate a straightforward mild thermal annealing procedure (50–80 °C) with no chemical treatments involved, to manipulate as-synthesized GO structures on a large scale by facilitating transformation of mixed  $sp^2$ – $sp^3$  hybridized GO phases into distinct oxidized and graphitic phases. With this approach, oxygen functionality is preserved, and we obtain large improvements in the optical and electronic properties of GO. We demonstrate a strong increase in the visible absorption characteristics compared with those of as-synthesized GO samples, and an opening up of optical gaps in the range 0.5–2.5 eV. We also show enhanced electronic conductivity, by up to four orders of magnitude, and photoluminescence (PL) modulation in annealed GO structures. To understand our experimental results, molecular dynamics (MD) and density functional theory (DFT) calculations were performed on a large set of realistic, disordered GO structures. We show that as-synthesized GO structures are metastable and

<sup>1</sup>Department of Materials Science and Engineering, Massachusetts Institute of Technology, Cambridge, Massachusetts 02139, USA, <sup>2</sup>The David H. Koch Institute for Integrative Cancer Research, Massachusetts Institute of Technology, Cambridge, Massachusetts 02139, USA, <sup>3</sup>Department of Materials Science and Engineering, University of California, Berkeley, California 94704, USA, <sup>4</sup>Department of Biological Engineering, Massachusetts Institute of Technology, Cambridge, Massachusetts 02139, USA, <sup>†</sup>These authors contributed equally. \*e-mail: belcher@mit.edu; jcg@mit.edu

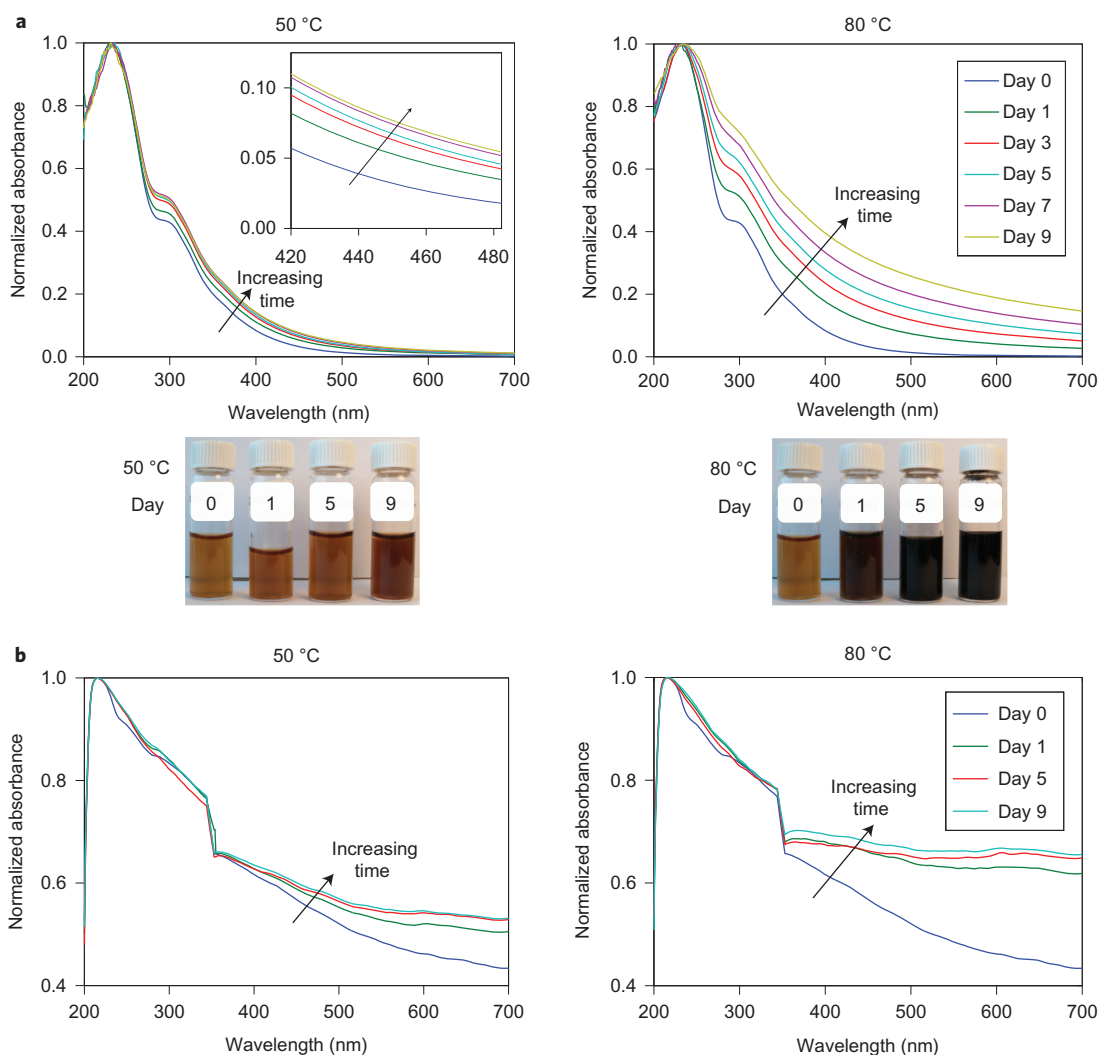


**Figure 1 | Improvement in the optical properties of annealed GO structures.** **a**, Normalized UV-vis absorption spectra of GO suspensions aged at 50 and 80 °C at different time intervals show increasing visible absorbance with thermal annealing. The inset in the 50 °C case shows the trend at a higher magnification (for clarity). Also shown are photographs that compare the colour change of GO suspensions under continuous annealing at 50 and 80 °C. **b**, UV-vis measurements on fd-GO samples show a similar increasing trend, but a much stronger visible absorbance with thermal annealing. The bump near 360 nm results from the change of detectors (from visible to ultraviolet).

undergo phase separation under the influence of temperature that drives oxygen diffusion by overcoming the associated kinetic barriers<sup>27–29</sup>. Taken together, our results shed light on the structural stability of GO and open new opportunities for large-scale processing of as-synthesized GO sheets in a wide range of applications.

## Results and discussion

GO sheets were synthesized by the Hummers method<sup>16</sup>. We performed thermal annealing studies on both GO suspensions and freeze-dried GO (fd-GO) samples to discount the effects of the solvent environment. GO suspensions were prepared by thoroughly exfoliating GO sheets in water (~0.5 wt% solids). Two stock solutions were prepared by diluting this solution (10×) and annealing for a course of nine days, one at 50 ± 1 °C and the other at 80 ± 1 °C in a temperature-controlled oven. We chose to perform annealing at two different temperatures so as to understand the impact of kinetics on the resulting phase-transformation processes. Aliquots were retrieved at regular intervals of one, three, five, seven and nine days, and stored in a vacuum desiccator at room temperature for further characterization. We also performed a similar annealing procedure

with fd-GO samples (see Methods and Supplementary Information for more details on sample preparation and characterization).

The evolution of the ultraviolet–visible (UV-vis) absorption spectra of GO suspensions with thermal annealing is shown in Fig. 1a. The as-prepared GO samples (day 0) showed typical characteristics of a main absorbance peak at ~230 nm, attributed to  $\pi$ - $\pi^*$  transitions of C=C in amorphous carbon systems, and broad absorption in the visible region. The main absorbance peak remained intact at ~230 nm on annealing at both 50 and 80 °C, in contrast to a clear red shift to ~260 nm reported in rGO samples<sup>30</sup>, which indicates no major reduction in covalently bonded oxygen at these temperatures. In addition, a broad shoulder at ~300 nm, attributed to  $n$ - $\pi^*$  transitions of C=O, was observed during the entire course of thermal annealing. Although a weak monotonic increment in the visible absorption was recorded with increasing annealing time at 50 °C, GO samples annealed continuously at 80 °C became strongly absorbing in the visible region, consistent with the stronger darkening of these GO samples. UV-vis absorption measurements on fd-GO samples yielded similar trends, but the observed effects were much stronger, as shown in Fig. 1b (also see Supplementary Fig. 1). To put these results in

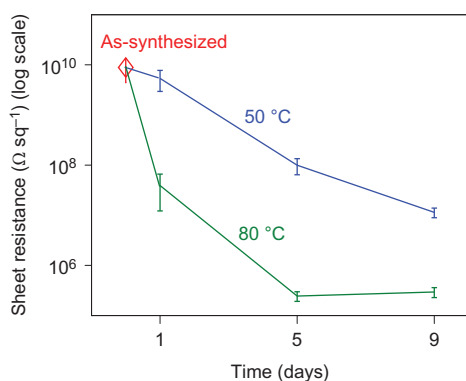


**Figure 2 | Enhanced electrical properties of annealed GO thin films.** Sheet resistances of GO thin films prepared from fd-GO samples annealed at 50 and 80 °C show a reduction by up to four orders of magnitude compared with the sheet resistance of the as-synthesized GO film. The error bars represent standard error of the mean from at least three different locations on the film.

perspective, in applications that involve light absorption, for example, we estimate that this increase in absorption corresponds to a significant 38% increase in the collection of photons in the wavelength range 350–800 nm, relative to as-synthesized GO (see Supplementary Fig. 2).

We investigated the electrical properties of thin films prepared from annealed GO samples using four-point probe transport measurements at room temperature. Films prepared from GO suspensions annealed at 50 °C showed no appreciable changes in the sheet-resistance values, and those from GO suspensions annealed at 80 °C showed a reduction by up to two orders of magnitude over the nine days, compared with as-synthesized GO samples ( $\sim 9 \times 10^9 \Omega \text{ sq}^{-1}$ , comparable to  $2\text{--}20 \times 10^9 \Omega \text{ sq}^{-1}$  reported previously<sup>27</sup>). In the case of films prepared from fd-GO samples, even further reductions in sheet resistance values were observed (Fig. 2). Significantly, low sheet resistances of  $\sim 3 \times 10^5 \Omega \text{ sq}^{-1}$  were measured in the case of fd-GO samples annealed for five and nine days at 80 °C, respectively, which are four orders of magnitude lower than the resistance of the as-synthesized GO samples and indicate superior electrical characteristics of annealed GO samples. These results are consistent with stronger changes observed in the UV-vis absorption data of fd-GO samples compared with those of GO suspensions (Fig. 1). Overall, this simple annealing procedure is effective in opening up new possibilities for fabricating thin-film devices with better electron-transport characteristics than those afforded by as-synthesized GO.

Although previous reports show enhanced electronic properties of GO under relatively low-temperature annealing, between 25 and 150 °C, combined with suitable chemical treatments<sup>21–23,31</sup>, such improvements come at the expense of oxygen content, which leads to the formation of rGO. In this work with a simple thermal annealing procedure, such control in optical and electronic properties is obtained without a compromise in the covalently bonded oxygen content, and without being subjected to any chemical treatments. To confirm this, we used thermogravimetric analysis (TGA) to monitor the level of reduction of our GO samples during the 80 °C annealing run (Fig. 3a). Although the annealed sample showed an expected slight weight loss ( $\sim 10\%$ ) over the entire course of annealing, attributed to the elimination of physisorbed and interlamellar water<sup>22</sup>, the thermogram of a typical as-synthesized GO sample shows an additional significant weight loss ( $\sim 32\%$ ) at an onset temperature of 150 °C, attributed to loss of covalently bonded oxygen from the GO sheets. This result shows that our GO samples are not reduced during the entire course of

thermal annealing, an observation additionally supported by X-ray photoelectron spectroscopy (XPS) measurements (see Supplementary Figs 3–5) and also in agreement with previous reports at these temperatures<sup>22,23</sup>. Collectively, these results suggest that the measured enhancement in optical and electronic properties does not come at the expense of oxygen atoms, which indicates that instead we are observing a distinct structural transformation inherent to GO.

To probe the fundamental mechanism responsible for the enhancement in the visible absorption and electrical conductivity of annealed GO samples, we carried out Fourier transform infrared (FTIR) spectroscopy measurements of GO samples during the annealing (Fig. 3b). Importantly, the recorded FTIR spectra clearly show the presence of oxygen functional groups for the entire course of annealing, which again confirms no major removal of oxygen groups from the graphene basal plane. In the case of samples prepared from GO suspensions annealed at 50 °C, the absorption peak at  $1,620 \text{ cm}^{-1}$ , assigned to the C=C skeletal vibrations of graphitic domains or the deformation vibration of intercalated water (scissor mode), remains more or less unchanged. In the case of annealing at 80 °C, this peak intensity decreases, which indicates a loss of intercalated water consistent with our TGA results, and a new peak appears with increasing intensity at  $1,580 \text{ cm}^{-1}$ , attributed to the formation of prominent graphitic domains in GO, consistent with previous studies<sup>20,22,23</sup>. Our FTIR measurements for fd-GO samples produced similar results, in addition to reflecting a stronger property enhancement in these samples (see Supplementary Fig. 6). Further, we observed a blue shift in our PL spectra measurements on GO suspensions annealed at 80 °C, as shown in Fig. 3c, which is attributed to the formation of confined graphene domains in GO<sup>30,32</sup>. The absence of a clear blue shift in the PL spectra of GO suspensions annealed at 50 °C correlates well with the FTIR spectra, and suggests a lack of prominent graphitic domains in these samples. XPS, Raman and additional PL analyses on annealed GO samples also support the clustering and formation of prominent graphitic domains (see Supplementary Figs 3–5 and 7–9). An increase in the stacking of GO sheets was also observed during annealing experiments, consistent with increasing  $\pi$ -conjugation and graphitization in the system (see Supplementary Fig. 10). Taken together, our experimental results suggest that an increasing formation of the graphitic phase in annealed GO samples (with no loss in oxygen content) is the critical factor responsible for the observed improvements in sheet properties.

As a means to probe directly the structural transformations taking place in GO, we performed Auger electron spectroscopy (AES) on as-synthesized and annealed GO thin films (see Methods). The presence of carbon and oxygen on the surface was detected using this technique (Fig. 4a). Figure 4b compares the elemental composition maps (oxygen-rich regions indicated by white spots) of as-synthesized and annealed GO thin films. Clearly, the as-synthesized GO film shows a uniform oxygen composition, and the annealed film shows sharper and segregated regions of oxygen. These results further establish the process of oxygen clustering and development of well-defined graphene-rich domains on annealing as-synthesized GO.

To interpret our experimental results, we propose that as-synthesized GO structures are metastable and have the potential to separate gradually into two distinct phases, graphitic and oxidized domains, under temperature-driven oxygen diffusion on the basal plane. Figure 4c shows a schematic of the phase separation process of an as-synthesized mixed  $sp^2$ – $sp^3$  GO phase into distinct graphitic and oxidized phases, which results in the formation of larger, well-defined graphitic domains confined in both dimensions. With longer annealing times, some of these domains may further interact and coalesce, which leads to percolation and greater

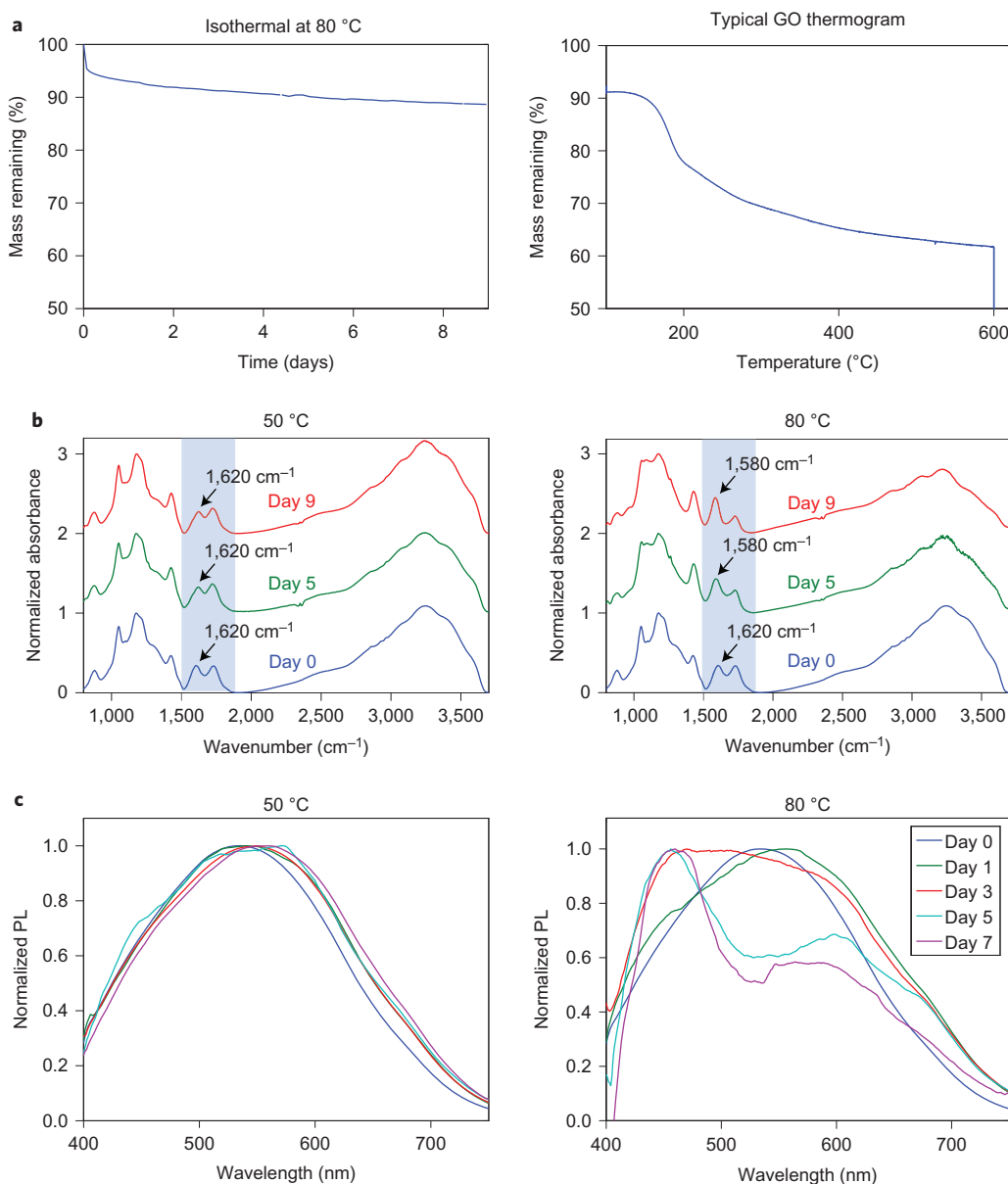


**Figure 3 | TGA, FTIR and PL spectra of annealed GO structures.** **a**, Recorded mass loss of a GO sample annealed at 80 °C for nine days shows only a slight reduction in mass (~10%) compared with a typical TGA thermogram of GO that shows an additional significant mass loss of ~32% because of the removal of oxygen from the basal plane. This indicates that GO is not reduced during the entire course of thermal annealing. **b**, FTIR spectra of the GO structures reveal increasing absorption intensities near 1,580 cm<sup>-1</sup> attributed to C=C bonds in the case of thermal annealing at 80 °C. This correlates with the increasing UV-vis absorbance and decreasing sheet resistance, which suggests the formation of prominent graphitic domains within the *sp*<sup>3</sup> matrix. **c**, PL emission from GO suspensions annealed at 50 and 80 °C show a blue shift in the peak PL emission wavelength in the latter case.

connectivity among neighbouring domains. Such prominent graphitic domains in an *sp*<sup>3</sup> matrix have been predicted to open up optical gaps in the visible<sup>30,32</sup>, which explains the increasing visible absorbance and blue shift in PL observed here. Furthermore, this model explains the increasing electrical conductivity of GO thin films with annealing because of graphitization and greater connectivity among the developed *sp*<sup>2</sup> domains, with no loss in the overall oxygen content.

To further support our hypothesis of a temporal phase separation, we carried out a combination of classical MD simulations based on reactive force fields (ReaxFF)<sup>33</sup> and DFT calculations. Model GO structures with different sizes of oxidized and graphitic domains (none, three and six graphene rows) were prepared with the oxygen concentration kept fixed to mimic the phase-separation process (Fig. 5a). Initially, the oxidized domains consisted of

randomly distributed epoxy and hydroxyl groups attached to both sides of the graphene sheet, consistent with previous work that shows the dominant presence of such functional groups in GO<sup>3,8,19</sup>. To account for local variations in oxygen concentration and fraction of functional groups on the GO sheet, we studied oxygen concentrations of 10 and 20 at% in the initial GO structures and prepared samples with epoxy to hydroxyl ratios of 3:2 and 2:3 (ref. 19). GO structures were then annealed at 300 K using MD simulations (see Methods for further details).

Our MD simulations produced GO structures that consisted of bare graphitic domains in conjunction with oxidized domains that largely contained epoxy and hydroxyl functional groups with a small amount of carbonyls and water molecules, consistent with previous computational work<sup>27</sup>. The generation of ten samples for each composition allows us to present meaningful averages of the

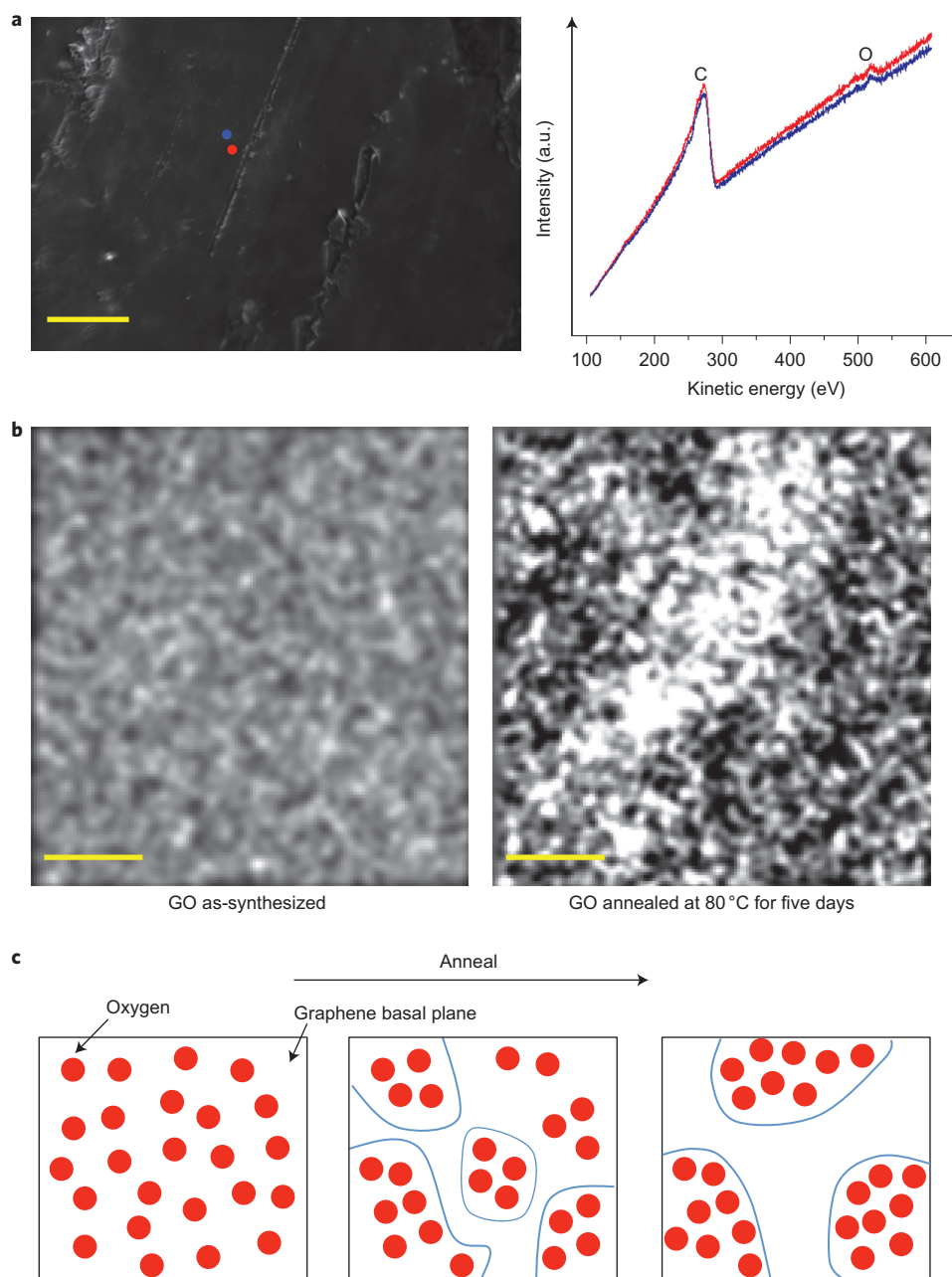


**Figure 4 | Direct evidence of phase separation in annealed GO structures.** **a**, SEM (left) and AES (right) of as-synthesized GO. The KLL peaks at 256 and 510 eV, respectively, show the presence of C and O. This was confirmed at two different locations (red and blue spots) on the film as indicated in the SEM image. Scale bar, 10  $\mu\text{m}$ . **b**, AES oxygen mapping of as-synthesized and annealed GO films. The white spots indicate oxygen-rich regions and the black spots indicate oxygen-poor regions or, in other words, carbon-rich regions. Scale bar, 2  $\mu\text{m}$ . **c**, Schematic depicting our proposed phase-separation process in as-synthesized GO structures. Synthetic protocols of GO structures lead to a mixed  $sp^2$ - $sp^3$  phase that has the potential to separate into two distinct oxidized and graphene phases through diffusion of oxygen atoms on the graphene basal plane under the influence of an external stimulus. a.u., arbitrary units.

computed properties. Figure 5b shows the total energy of the phase-separated GO structures computed from our MD simulations (internal energies at 300 K). We observe that the total energies decrease with increasing phase separation, that is, with increasing graphitic domain size, which suggests that the process of phase separation is thermodynamically favourable in GO structures. Additional calculations performed using chemically homogeneous and ordered phases of GO indicate similar trends and favourability of the phase-separation process (see Supplementary Fig. 11). We attribute this favourability to strain compensation and hence strain relief in the GO structures. For instance, although two isolated oxygen groups attached on either side of the graphene sheet increase

strains in their vicinity, the same oxygen groups can partially cancel these strains when present in proximity to one another, and thus favour phase separation and clustering of oxygen atoms on graphene<sup>34–37</sup>.

A key mechanism involved in the phase-separation process during annealing is the diffusion of epoxy and hydroxyl functional groups along the graphene basal plane. Our calculations show that diffusion of an isolated epoxy group is limited by an activation barrier of 0.83 eV, and the barrier for diffusion of an isolated hydroxyl group is 0.30 eV, much lower than that in the epoxy case (see Fig. 5c). Although diffusion of oxygen atoms at room temperature has been observed in GO multilayers previously, the

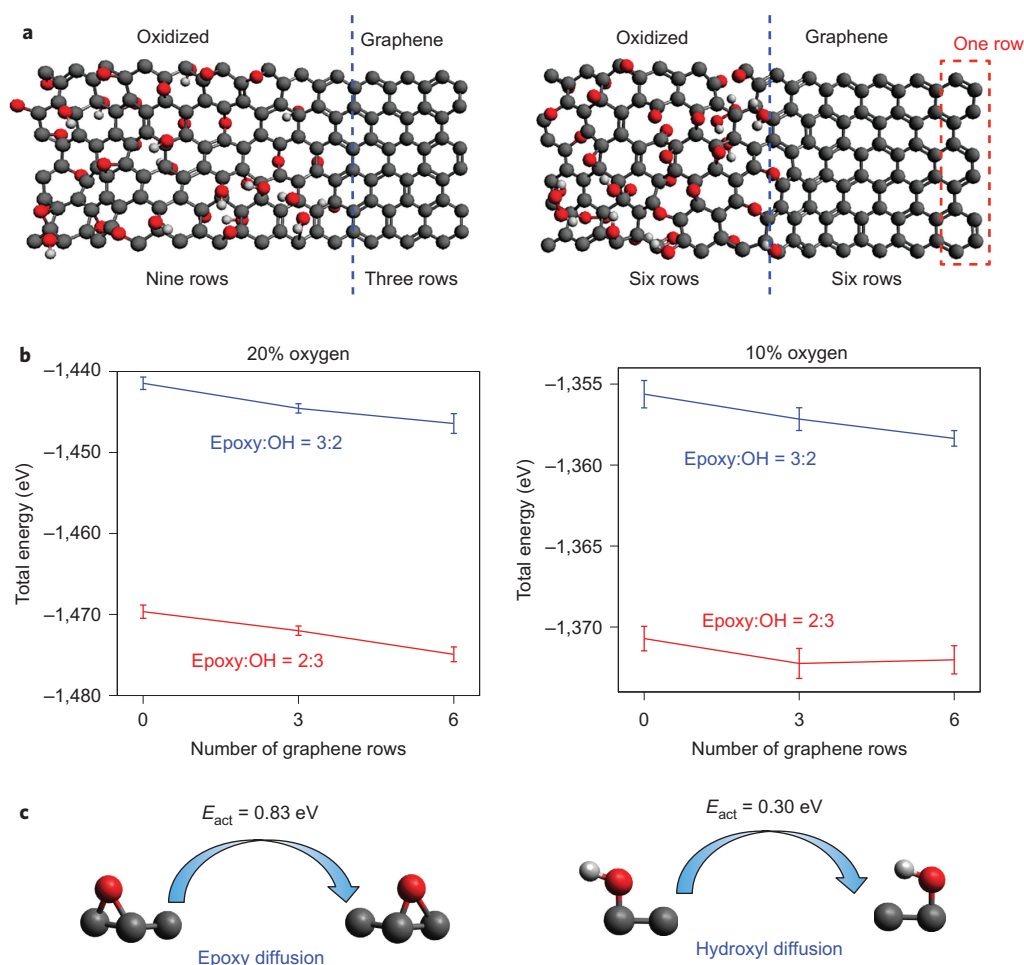


**Figure 5 | Favourable energetics of phase separation predicted by atomistic modelling.** **a**, Representative model GO structures used to compute the energetics of the phase-separation process. Each structure consists of two distinct oxidized and graphene phases with different domain sizes. Carbon, oxygen and hydrogen are represented as grey, red and white spheres, respectively. **b**, Total energy values of phase-separated GO structures as a function of the graphene domain size for different oxygen contents (in at%) and epoxy to hydroxyl functional group ratios. The total energies decrease on phase separation, which indicates the process to be thermodynamically favourable. In each plot, the results are obtained by averaging over ten GO structures for each data point, and the error bars shown represent the standard error of the mean calculated for the same set of structures. **c**, Computed activation barriers for the diffusion of epoxy and hydroxyl functional groups on the graphene basal plane.

structural changes were discernible only after months, which implies extremely low diffusion rates<sup>27</sup>. Using the Arrhenius formula  $k = k_0 \exp(-E_{act}/k_B T)$ , where  $E_{act}$  is the computed activation barrier and  $k_0$  is the attempt frequency (assumed to be constant), we estimate the hydroxyl and epoxy diffusion to increase by one and two orders of magnitude, respectively, at 80 °C (353 K) compared with their diffusion at room temperature (300 K), which correlates well to the fact that structural changes were observed over 1–5 days in our work, rather than the months for reported stock solutions preserved at room temperature, which hence warrant the application of external stimuli, such as elevated temperatures, to activate these structural changes.

We carried out additional analyses to estimate the range of domain sizes in annealed GO samples. Analogous to the case of phase separation in hybridized carbon boron nitride monolayers<sup>38</sup>, our calculations also indicate that larger graphitic domains are thermodynamically preferred to decrease the number of interfaces and the associated interfacial energy between oxidized and graphitic domains (see Supplementary Fig. 11). To understand the structural evolution of GO on annealing, we first note that the as-synthesized GO structure consists of two distinct features: (1) small  $sp^2$  fragments (or chains) that correspond to no specific structure and (2)

larger unoxidized graphitic domains on the order of  $\sim 3$  nm in size<sup>30</sup>. On progressively annealing GO, we expect the small  $sp^2$  fragments to interact and coalesce (or, in other words, undergo the process of phase separation), which leads to well-defined graphitic domains. On the basis of Raman and additional PL spectra from GO thin films, we conclude that most of the domains are on the order of 1–2 nm (see Supplementary Figs 7–9) and are mainly responsible for the observed blue shift in the PL (2–2.5 eV).

In parallel, it is reasonable to expect that the  $\sim 3$  nm domains already present in as-synthesized GO will grow further on annealing. We expect these domain sizes to extend from  $\sim 3$  nm to tens of nanometres, similar to the range of domain sizes observed in carbon boron nitride monolayers<sup>38</sup>. Our DFT calculations show that such large domains formed within the  $sp^3$  matrix open up optical gaps continuously up to 2 eV (see Supplementary Fig. 12), which helps explain the continuous increase in the optical absorption spectra in both the visible and infrared regions. Further, these estimates also explain why certain regions are relatively oxygen rich compared with other regions in our AES maps. Although formation of such larger domains on the order of tens of nanometres requires considerable diffusion of oxygen groups, we found that such mean diffusion lengths can, nevertheless, be

achieved at the temperatures considered in this work (see Supplementary Section 5). Although we show these results for our as-synthesized GO samples with an oxygen content of ~30%, we expect these domain sizes to be tunable depending on the oxygen concentration, temperature and anneal time, and so provide additional opportunities for controlling the properties of oxidized graphene.

## Conclusion

In summary, we present a highly scalable, easily controllable, mild thermal annealing procedure that involves no chemical treatments to manipulate as-synthesized GO suspensions and solids through a phase-separation process. We demonstrate that such phase-transformation processes have significant impact on the sheet properties by (1) making GO strongly absorbing in the visible region, (2) reducing the electrical resistance by four orders of magnitude and (3) producing a blue shift in PL emission, without compromising the oxygen content. Atomistic calculations support our experimental results and show that the phase separation of the mixed  $sp^2$ - $sp^3$  hybridized GO phase into prominent oxidized and graphitic domains is energetically favourable and kinetically accelerated at slightly elevated temperatures compared with room temperature. In addition to shedding light on the thermal stability of GO nanostructures when employed in devices that operate above room temperature, these results open up novel opportunities for bulk processing of as-synthesized GO structures, and highlight pathways to tune the sheet properties of GO for their application in next-generation functional devices.

## Methods

**Synthesis of GO.** GO was prepared from synthetic graphite powder (~325 mesh, 99.9%, Alfa Aesar) using the Hummers approach<sup>16</sup>. The yellowish-brown filter cake obtained was suspended in 320 ml of water to give a GO suspension of ~0.5 wt% solids. The suspension was put in a sealed glass bottle and kept in a vacuum desiccator for long-term storage. It was observed that the stock suspension is stable at room temperature, without the addition of any surfactant.

**Preparation of fd-GO samples.** To study the effects of long-term thermal annealing on GO alone, and discount the effects of the solvent environment, we prepared dried samples from the stock suspension. The stock suspension was diluted to 10 $\times$  and 1 ml of this diluted suspension was taken in several Eppendorf tubes, which were solidified rapidly by plunging into liquid nitrogen. The frozen samples were put in a lyophilizer (Labconco FreeZone 2.5 Plus), and kept at 0.008 mbar pressure for a day for complete extraction of the water content from the samples. These samples were stored in a vacuum desiccator.

**Time-course annealing of GO samples.** We studied the effects of thermal annealing on both GO suspensions and fd-GO samples. For GO suspensions, 1 ml of the 10 $\times$  diluted stock solution was taken in ten Eppendorf tubes. For the fd-GO samples, the lyophilized samples were used as is in ten Eppendorf tubes. One batch of five samples (both suspension and solids) was placed in a vacuum oven at 50 °C, and another similar batch at 80 °C. Both batches were started simultaneously at  $t = 0$ . Then, at  $t = 1, 3, 5, 7$  and 9 days, we retrieved one Eppendorf tube from each oven (both solid and liquid samples), and these were stored in a vacuum desiccator at room temperature for further characterization.

**UV-vis absorbance spectroscopy.** GO suspensions obtained from annealing experiments were subjected to a vortex treatment and further sonicated for 20 minutes. They were then diluted to 160 $\times$  (of the stock suspension) for absorbance measurements. The sample (100  $\mu$ l) was taken in a glass cuvette of path length 1 cm. UV-vis absorbance was measured using a DU-800 Spectrophotometer (Beckman Coulter) with respect to a water (blank) baseline. The scan range was 200–1,100 nm at a scan rate 600 nm min<sup>-1</sup>. For the UV-vis absorption measurements on fd-GO samples, we used a Cary 300 spectrophotometer (Agilent Technologies) with a solid-state sample accessory with  $z$ -height adjustment, operating in diffuse reflectance mode. The fd-GO samples were scanned from 200 to 800 nm at a scan rate of 1 nm s<sup>-1</sup>. The reflectance measurements were converted into corresponding absorbance data after suitable background subtraction.

**Four-point probe measurements.** Electrical transport measurements of GO films prepared from annealed GO samples were carried out using a four-point probe technique (Model 2525, The Micromanipulator Company) at room temperature. GO samples were drop-cast into 1 cm<sup>2</sup> area films on an insulating glass substrate. Measurements were taken by varying the applied voltage from -1 to +1 V.

**Infrared spectroscopy.** GO suspensions obtained from annealing experiments were freeze dried and the FTIR spectrum (800–4,000 cm<sup>-1</sup>) was measured using a Thermo Fisher Continuum FTIR Microscope in the transmission mode. A spot size of 100  $\mu$ m was used. The transmission measurements were converted into corresponding absorbance data and a suitable five-point baseline correction was applied to all spectra.

**PL measurements.** PL from the GO samples was measured using a NanoLog spectrofluorometer (HORIBA Jobin Yvon). The GO samples were diluted in water to 500 $\times$  the stock concentration. A continuous-wave xenon lamp with a monochromator was used for the excitation source and the samples were excited at 350 nm. The fluorescence was measured in the range 400–750 nm, using a FluoroHub single photon counter (HORIBA Jobin Yvon), with an integration time of 0.1 s nm<sup>-1</sup>.

**TGA.** We characterized the thermal properties of GO by TGA (TA Instruments Q500 TGA). GO solids were equilibrated initially at 30 °C for 30 minutes, followed by a ramp-up to 80 °C where they were held isothermally for nine days to record mass loss during the annealing run. Typical GO thermograms were obtained by similar equilibration, followed by a ramp-up to 800 °C. All measurements were taken at a nitrogen gas flow rate of 40 ml min<sup>-1</sup> and a ramp rate of 5 °C min<sup>-1</sup> was used.

**Nano-AES measurements.** Auger spectroscopy was performed using a field emission electron source and a multichannel detector at ultrahigh vacuum (2–5  $\times 10^{-10}$  mbar) with 100 nm spatial resolution. Increasing resolution beyond this limit resulted in weaker signal collection and poor elemental contrast. As a result, this technique provides direct evidence of oxygen clustering and/or segregation, but to obtain quantitative information on the domain size is rather difficult. A series of Auger spectra were measured on several different regions with a minimum scan area of 3  $\times$  3  $\mu$ m. The AES scanning was performed to detect the oxygen concentration. To eliminate the native oxide contribution on conventional substrates, such as SiO<sub>2</sub>, Si and Al<sub>2</sub>O<sub>3</sub>, GO was transferred onto non-oxidizing MoS<sub>2</sub> substrates.

**Computational methods.** MD simulations used to prepare realistic GO structures were carried out using the LAMMPS package<sup>39</sup> with the ReaxFF reactive force field, chosen here for its ability to describe accurately the bond-breaking and bond-formation events in hydrocarbon systems<sup>33</sup>. We employed a time step of 0.25 fs and the NVT Berendsen thermostat<sup>19</sup>. To assess the energetics of the phase-separation process into oxidized and graphitic domains, we considered 3  $\times$  1.3 nm periodic graphene sheets with different oxidized and graphitic domain sizes. The oxidized domains contained randomly distributed epoxy and hydroxyl groups<sup>40,41</sup>. The temperature of the GO sheets was increased from 10 K to 300 K over a time interval of 250 fs. The system was then annealed at 300 K for 250 ps to allow for structural stabilization. Such MD thermal anneal runs have been employed previously by us and other groups to generate both GO and reduced GO structures<sup>19,27,41</sup>.

In all the DFT calculations presented in this work, the structures were relaxed to less than 0.03 eV  $\text{\AA}^{-1}$  residual atomic forces using DFT with a plane-wave basis set as implemented in the VASP package<sup>42,43</sup>. We used the projector augmented wave method to describe the core electrons<sup>44</sup> and the Perdew–Burke–Ernzerhof exchange-correlation functional<sup>45</sup>. Isolated epoxy and hydroxyl groups were modelled on a periodic graphene sheet with 120 carbon atoms using a gamma-point  $k$ -grid. The wave function and charge density were expanded in plane waves with a wavefunction kinetic energy cutoff of 500 eV. A vacuum region of 16  $\text{\AA}$  was used in the direction normal to the sheets. To compute the activation energies used to determine the kinetics of oxygen diffusion, we employed nudged elastic band calculations as implemented in VASP with 9–13 image structures between the reactant and the product.

Received 13 May 2013; accepted 8 November 2013;  
published online 15 December 2013

## References

- Eda, G., Fanchini, G. & Chhowalla, M. Large-area ultrathin films of reduced graphene oxide as a transparent and flexible electronic material. *Nature Nanotechnol.* **3**, 270–274 (2008).
- Eda, G. & Chhowalla, M. Chemically derived graphene oxide: towards large-area thin-film electronics and optoelectronics. *Adv. Mater.* **22**, 2392–2415 (2010).
- Loh, K. P., Bao, Q., Eda, G. & Chhowalla, M. Graphene oxide as a chemically tunable platform for optical applications. *Nature Chem.* **2**, 1015–1024 (2010).
- Kamat, P. V. Graphene-based nanoassemblies for energy conversion. *J. Phys. Chem. Lett.* **2**, 242–251 (2011).
- Yun, J. M. *et al.* Solution-processable reduced graphene oxide as a novel alternative to PEDOT:PSS hole transport layers for highly efficient and stable polymer solar cells. *Adv. Mater.* **23**, 4923–4928 (2011).
- Xu, B. *et al.* What is the choice for supercapacitors: graphene or graphene oxide? *Energy Environ. Sci.* **4**, 2826–2830 (2011).
- Zhu, X., Zhu, Y., Murali, S., Stoller, M. D. & Ruoff, R. S. Nanostructured reduced graphene oxide/Fe<sub>2</sub>O<sub>3</sub> composite as a high-performance anode material for lithium ion batteries. *ACS Nano* **5**, 3333–3338 (2011).

8. Gao, W., Alemany, L. B., Ci, L., & Ajayan, P. M. New insights into the structure and reduction of graphite oxide. *Nature Chem.* **1**, 403–408 (2009).
9. Johns, J. E. & Hersam, M. C. Atomic covalent functionalization of graphene. *Acc. Chem. Res.* **46**, 77–86 (2013).
10. Su, C. *et al.* Probing the catalytic activity of porous graphene oxide and the origin of this behaviour. *Nature Commun.* **3**, 1298–1306 (2012).
11. Pyun, J. Graphene oxide as catalyst: application of carbon materials beyond nanotechnology. *Angew. Chem. Int. Ed.* **50**, 46–48 (2011).
12. Ramanathan, T. *et al.* Functionalized graphene sheets for polymer nanocomposites. *Nature Nanotechnol.* **3**, 327–331 (2008).
13. Potts, J. R., Dreyer, D. R., Bielawski, C. W. & Ruoff, R. S. Graphene-based polymer nanocomposites. *Polymer* **52**, 5–25 (2011).
14. Kamat, P. V. Graphene-based nanoarchitectures. Anchoring semiconductor and metal nanoparticles on a two-dimensional carbon support. *J. Phys. Chem. Lett.* **1**, 520–527 (2010).
15. Lin, Y. *et al.* Dramatically enhanced photoresponse of reduced graphene oxide with linker-free anchored CdSe nanoparticles. *ACS Nano* **4**, 3033–3038 (2010).
16. Hummers, W. S. & Offeman, R. E. Preparation of graphitic oxide. *J. Am. Chem. Soc.* **80**, 1339 (1958).
17. Szabo, T. *et al.* Evolution of surface functional groups in a series of progressively oxidized graphite oxides. *Chem. Mater.* **18**, 2740–2749 (2006).
18. Hunt, A. *et al.* Epoxide speciation and functional group distribution in graphene oxide paper-like materials. *Adv. Funct. Mater.* **22**, 3950–3957 (2012).
19. Hossain, Z. *et al.* Chemically homogeneous and thermally reversible oxidation of epitaxial graphene. *Nature Chem.* **4**, 305–309 (2012).
20. Bagri, A. *et al.* Structural evolution during the reduction of chemically derived graphene oxide. *Nature Chem.* **2**, 581–587 (2010).
21. Feng, H., Cheng, R., Zhao, X., Duan, X. & Li, J. A low-temperature method to produce highly reduced graphene oxide. *Nature Commun.* **5**, 1539–1545 (2013).
22. Fan, X. *et al.* Deoxygenation of exfoliated graphite oxide under alkaline conditions: a green route to graphene preparation. *Adv. Mater.* **20**, 4490–4493 (2008).
23. Rourke, J. P. *et al.* The real graphene oxide revealed: stripping the oxidative debris from the graphene-like sheets. *Angew. Chem. Int. Ed.* **50**, 3173–3177 (2011).
24. Liao, K. H. *et al.* Aqueous only route toward graphene from graphite oxide. *ACS Nano* **5**, 1253–1258 (2011).
25. Wei, Z. *et al.* Nanoscale tunable reduction of graphene oxide for graphene electronics. *Science* **328**, 1373–1376 (2010).
26. Mattson, E. C. *et al.* Evidence of nanocrystalline semiconducting graphene monoxide during thermal reduction of graphene oxide in vacuum. *ACS Nano* **5**, 9710–9717 (2011).
27. Kim, S. *et al.* Room-temperature metastability of multilayer graphene oxide films. *Nature Mater.* **11**, 544–549 (2012).
28. Suarez, A. M., Radovic, L. R., Bar-Ziv, E. & Sofo, J. O. Gate-voltage control of oxygen diffusion on graphene. *Phys. Rev. Lett.* **106**, 146802 (2011).
29. Solenov, D. & Velizhanin, K. A. Adsorbate transport on graphene by electromigration. *Phys. Rev. Lett.* **109**, 095504 (2012).
30. Eda, G. *et al.* Blue photoluminescence from chemically derived graphene oxide. *Adv. Mater.* **22**, 505–509 (2010).
31. Jung, I., Dikin, D. A., Piner, R. D. & Ruoff, R. S. Tunable electrical conductivity of individual graphene oxide sheets reduced at low temperatures. *Nano Lett.* **8**, 4283–4287 (2008).
32. Chien, C. T. *et al.* Tunable photoluminescence from graphene oxide. *Angew. Chem. Int. Ed.* **51**, 6662–6666 (2012).
33. Van Duin, A. C. T., Dasgupta, S., Lorant, F. & Goddard, W. A. ReaxFF: A reactive force field for hydrocarbons. *J. Phys. Chem. A* **105**, 9396–9409 (2001).
34. Wang, L. *et al.* Stability of graphene oxide phases from first-principles calculations. *Phys. Rev. B* **82**, 2–5 (2010).
35. Nguyen, M. T., Erni, R. & Passerone, D. Two-dimensional nucleation and growth mechanism explaining graphene oxide structures. *Phys. Rev. B* **86**, 115406 (2012).
36. Topsakal, M. & Ciraci, S. Domain formation on oxidized graphene. *Phys. Rev. B* **86**, 205402 (2012).
37. Huang, B., Xiang, H., Xu, Q. & Wei, S. H. Overcoming the phase inhomogeneity in chemically functionalized graphene: the case of graphene oxides. *Phys. Rev. Lett.* **110**, 085501 (2013).
38. Ci, L. *et al.* Atomic layers of hybridized boron nitride and graphene domains. *Nature Mater.* **9**, 430–435 (2010).
39. Plimpton, S. Fast parallel algorithms for short-range molecular dynamics. *J. Comput. Phys.* **117**, 1–19 (1995).
40. Paci, J. T., Belytschko, T. & Schatz, G. C. Computational studies of the structure, behavior upon heating, and mechanical properties of graphite oxide. *J. Phys. Chem. B* **111**, 18099–18111 (2007).
41. Kumar, P. V., Bernardi, M. & Grossman, J. C. The impact of functionalization on the stability, work function, and photoluminescence of reduced graphene oxide. *ACS Nano* **7**, 1638–1645 (2013).
42. Kresse, G. & Furthmüller, J. Efficient iterative schemes for *ab-initio* total-energy calculations using a plane-wave basis set. *Phys. Rev. B* **54**, 11169–11186 (1996).
43. Kresse, G. Efficiency of *ab-initio* total energy calculations for metals and semiconductors using a plane-wave basis set. *Comput. Mater. Sci.* **6**, 15–50 (1996).
44. Kresse, G. & Joubert, D. From ultrasoft pseudopotentials to the projector augmented-wave method. *Phys. Rev. B* **59**, 1758 (1999).
45. Perdew, J., Burke, K. & Ernzerhof, M. Generalized gradient approximation made simple. *Phys. Rev. Lett.* **77**, 3865–3868 (1996).

### Acknowledgements

The authors dedicate this paper to the memory of S. Collier for his caring service to the Massachusetts Institute of Technology (MIT) community and for his sacrifice in defending the MIT campus in the line of duty. P.V.K. is grateful to Eni for financial support via the Solar Frontiers Program at MIT. P.V.K. and J.C.G. thank the Texas Advanced Computer Sector Stampede system for computational resources. This study was supported in part by the Institute for Collaborative Biotechnologies through grant W911NF-09-0001 from the US Army Research Office. Work at the Molecular Foundry was supported by the Office of Science, Office of Basic Energy Sciences, of the US Department of Energy under Contract No. DE-AC02-05CH11231. N.M.B. and P.V.K. are grateful for the use of the Materials Analysis Shared Experimental Facilities at the Center for Materials Science and Engineering at MIT, and thank T. McClure, E. Shaw, T. Kucharski, J. Qi, G. Zhang, J. Ohmura and A. Maurano for assistance with experiments.

### Author contributions

P.V.K., N.M.B., A.M.B. and J.C.G. conceived and designed the experiments, P.V.K. and N.M.B. performed the experiments, calculations and co-wrote the manuscript with input from J.C.G. and A.M.B., and S.T. and J.W. performed AES, and contributed to Raman and PL mapping.

### Additional information

Supplementary information is available in the [online version](#) of the paper. Reprints and permissions information is available online at [www.nature.com/reprints](http://www.nature.com/reprints). Correspondence and requests for materials should be addressed to A.M.B. and J.C.G.

### Competing financial interests

The authors declare no competing financial interests.